"Giant Surfactants" Created by the Fast and Efficient Functionalization of a DNA Tetrahedron with a Temperature-Responsive Polymer

Wilks, Thomas R.; Bath, Jonathan; de Vries, Jan Willem; Raymond, Jeffery E.; Herrmann, Andreas; Turberfield, Andrew J.; O'Reilly, Rachel K.; O’Reilly, Rachel K.

Published in:
Acs Nano

DOI:
10.1021/nn402642a

'Giant Surfactants' Created by the Fast and Efficient Functionalization of a DNA Tetrahedron with a Temperature-Responsive Polymer

Thomas R. Wilks,[†] *Jonathan Bath,*[‡] *Jan Willem de Vries,*[§] *Jeffery E. Raymond,*[‖] *Andreas Herrmann,*[§] *Andrew J. Turberfield*[‡] *and Rachel K. O'Reilly*[†]*

[†] Department of Chemistry, University of Warwick, Coventry, CV4 7AL, UK.

[‡] Department of Physics, University of Oxford, Clarendon Laboratory, Parks Road, Oxford, OX1 3PU, UK.

[§] Department of Polymer Chemistry, Zernike Institute for Advanced Materials, University of Groningen, Nijenborgh 4, 9747 AG Groningen, The Netherlands.

[‖] Laboratory for Synthetic-Biologic Interactions, Texas A&M University, POB 30012, College Station, TX 77842-3012, USA.

* Address all correspondence to rachel.oreilly@warwick.ac.uk

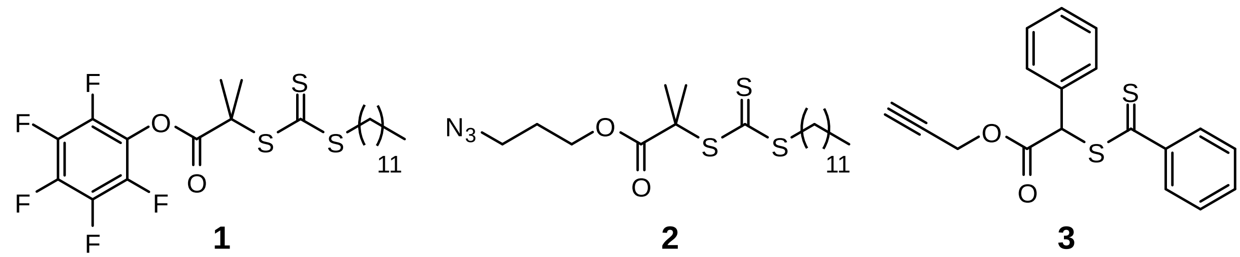

Figure S1. Structures of CTAs **1-3**.

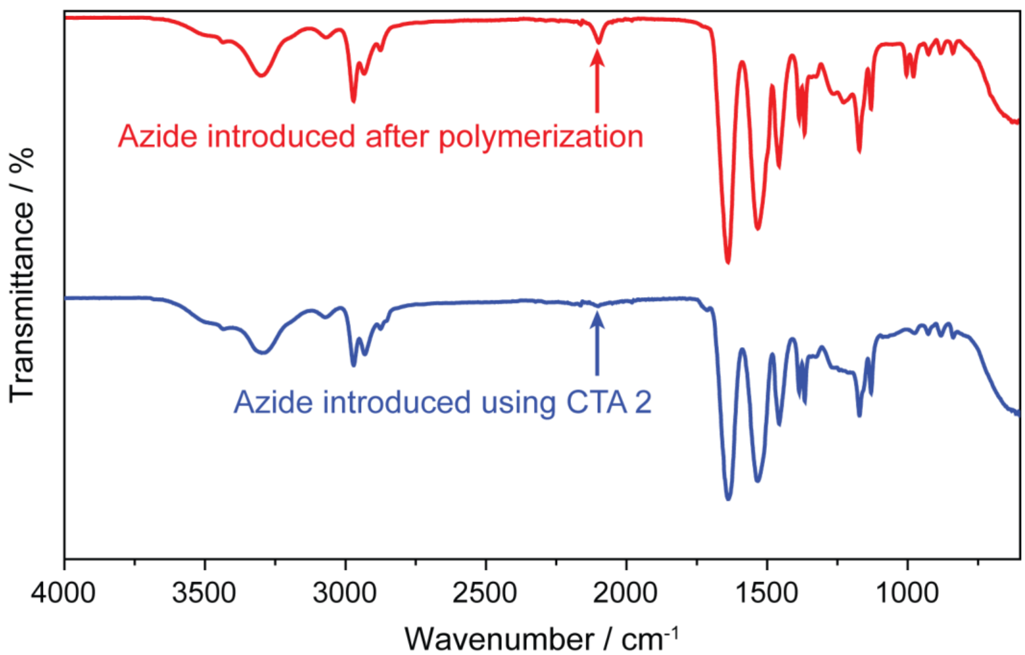

Figure S2. FTIR spectra of azide-terminated poly(NIPAM) synthesized by (top, red trace) post-polymerization functionalization, and (bottom, blue trace) by polymerization of NIPAM with azide-containing CTA 2. The arrows indicate the location of the peak due to the azide asymmetric stretch.

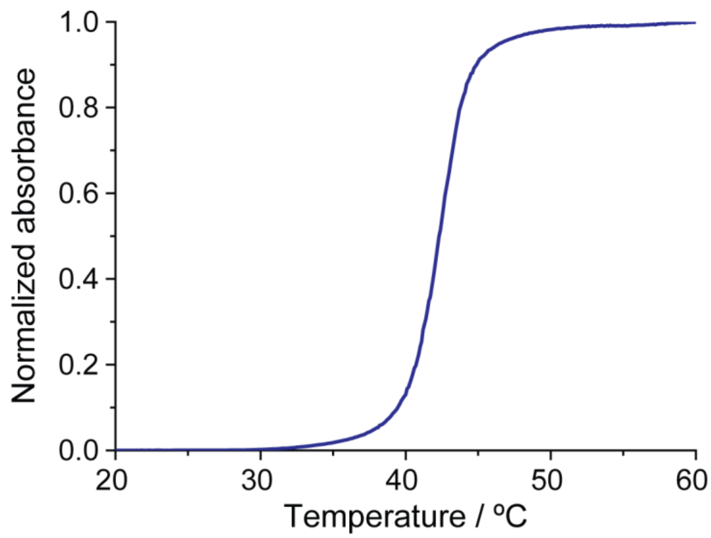

Figure S3. Determination of the cloud point of poly(NIPAM)$_{45}$ by UV-vis spectroscopy. The cloud point was taken as the temperature at which the normalized absorbance at 500 nm was 0.5.

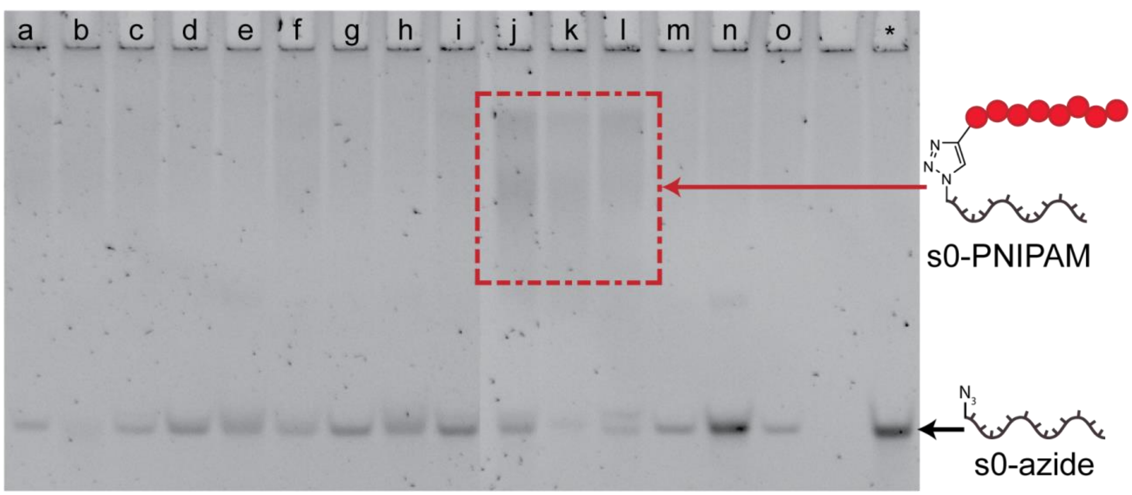

Figure S4. 15 % native PAGE of crude reaction mixtures testing different catalyst combinations for the CuAAC reaction between s0-azide DNA and alkyne-functionalized poly(NIPAM), stained with SyBr GOLD and visualized under UV trans-illumination. Lanes a-o: crude reaction mixtures as detailed in Table S1; lane *: pure s0-azide DNA.

Table S1. Catalyst combinations tested for the CuAAC reaction between azide-functionalized DNA and alkyne functionalized poly(NIPAM).

Experiment	Catalyst	Solvent
a		DMF
b	Cu(I)Br/THPTA	THF
c		DMSO
d		DMF
e	Cu(I)Br/PMDETA	THF
f		DMSO
g		DMF
h	Cu(I)Br/NHPMI/TEA	THF
i		DMSO
j		DMF
k	$CuI \cdot P(OEt)_3$	THF
l		DMSO
m		DMF
n	Cu(I)Br/BiPy/TEA	THF
o		DMSO

Table S2. Reactions conditions used in catalyst optimization for DNA-polymer conjugation *via* CuAAC.

Experiment	[Polymer] / µM	[CuI · P(OEt)$_3$] / µM	Solvent
a	1000	1000	DMF
b	5000	1000	DMF
c	1000	5000	DMF
d	5000	5000	DMF
e	1000	1000	DMSO
f	5000	1000	DMSO
g	1000	5000	DMSO
h	5000	5000	DMSO
i	1000	1000	MeCN
j	5000	1000	MeCN
k	1000	5000	MeCN
l	5000	5000	MeCN
m	1000	1000	NMP
n	5000	1000	NMP
o	1000	5000	NMP
p	5000	5000	NMP
q	1000	1000	THF
r	5000	1000	THF
s	1000	5000	THF

t	5000	

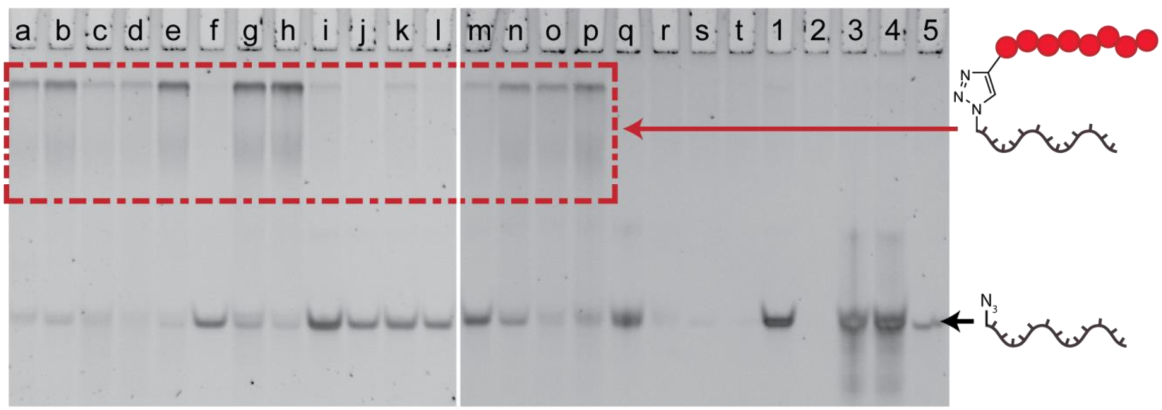

Figure S5. Optimization of catalyst conditions for the synthesis of DNA-polymer conjugates *via* CuAAC. Lanes a-t: reaction mixtures as detailed in **Table S2**; lane 1: s0-azide DNA + alkyne polyNIPAM (no catalyst); lane 2: alkyne polyNIPAM; lane 3: s0-azide DNA + CuI · $P(OEt)_3$; lane 4: s0-amine DNA + alkyne polyNIPAM + CuI · $P(OEt)_3$; lane 5: s0-azide DNA.

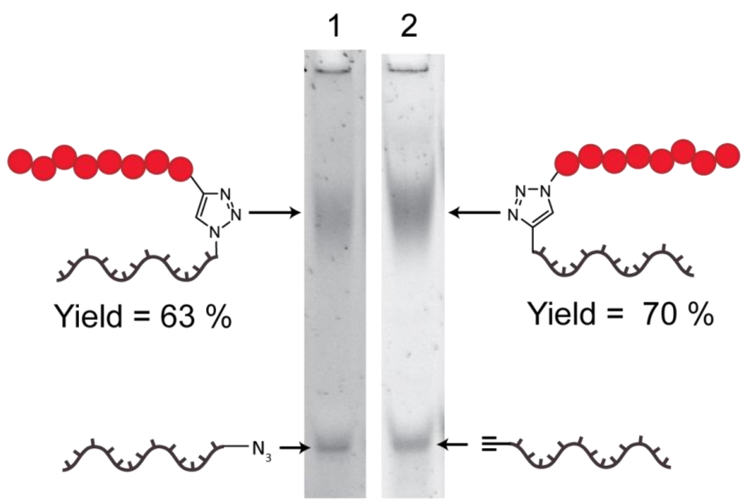

Figure S6. 15 % native PAGE analysis of the crude reactions mixtures of (1) azide-functionalized DNA reacting with alkyne-functionalized poly(NIPAM), and (2) alkyne-functionalized DNA reacting with azide-functionalized poly(NIPAM).

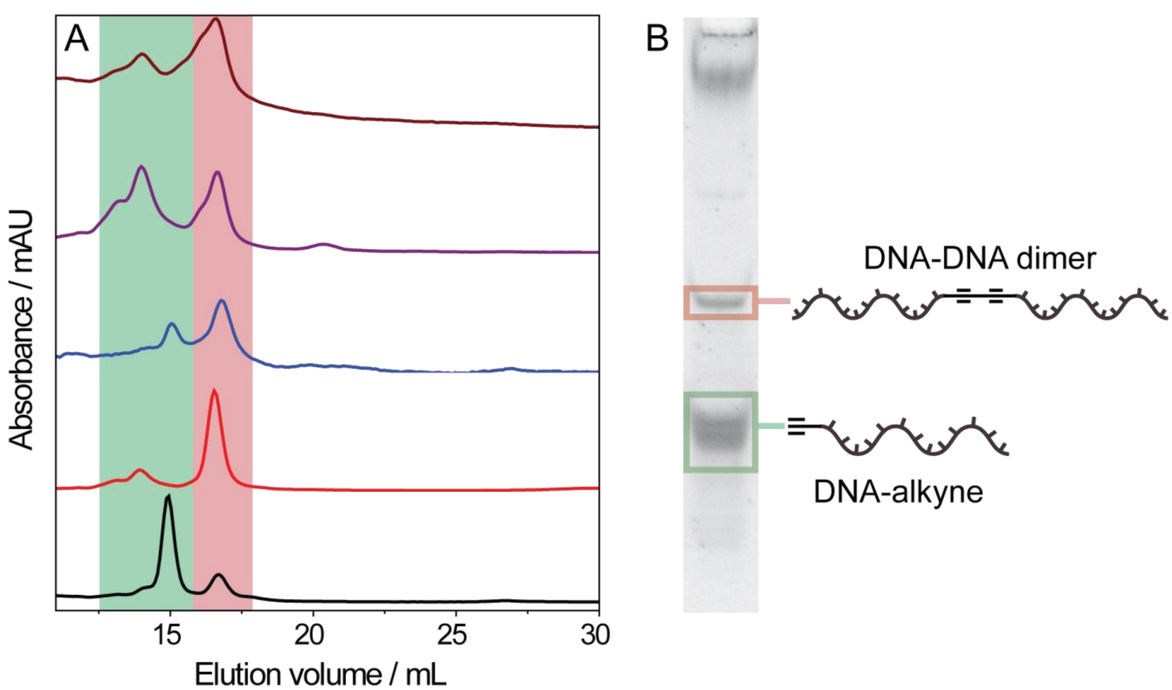

Figure S7. A: HPLC chromatograms showing DNA starting material (green) and the Glaser coupling product (red). The conditions for each reaction were the same except for the polymers used, which were (top to bottom): poly(styrene), poly(NIPAM), poly(styrene), poly(dimethylacrylamide), poly(NIPAM). **B**: 15 % native PAGE showing the presence of the Glaser coupling product.

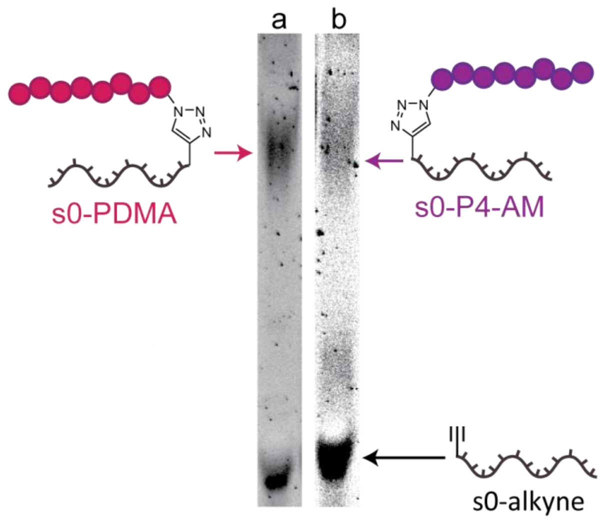

Figure S8. 15 % native PAGE analysis of the crude reaction mixtures in the synthesis of (a) s0-poly(dimethylacrylamide) and (b) s0-poly(4-acryloyl morpholine). Densiometric analysis estimated the yield to be around 50 % in each case.

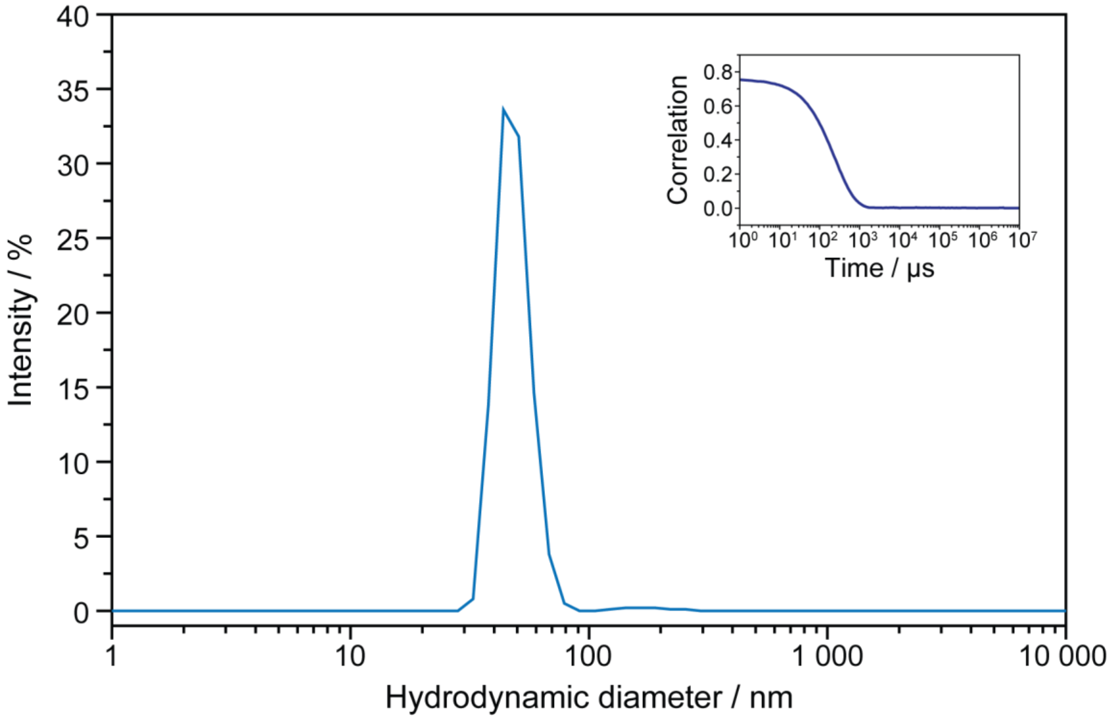

Figure S9. DLS analysis of the solution of s0−poly(styrene) nanoparticles.

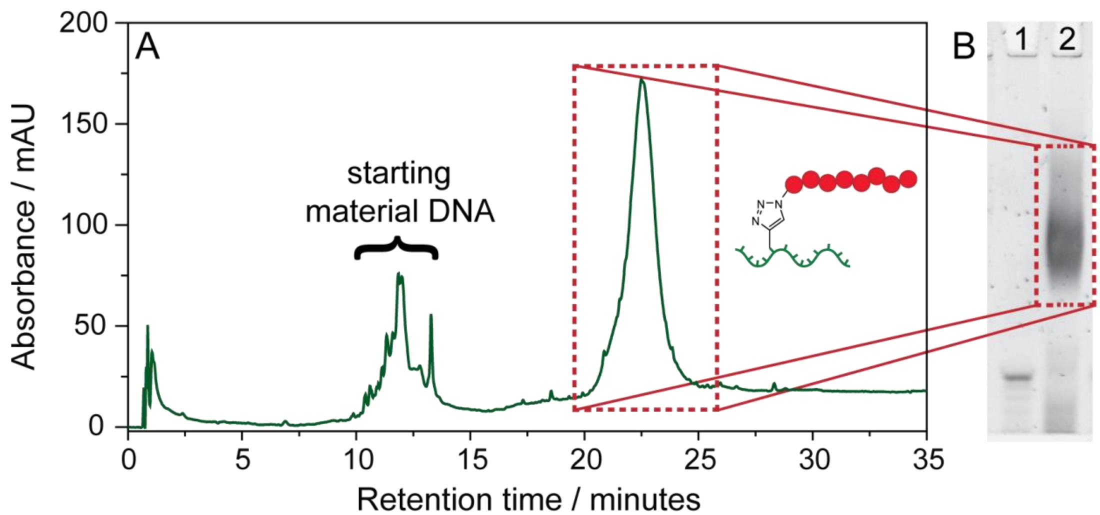

Figure S10. A: HPLC chromatogram of the crude reaction mixture in the synthesis of the s2-poly(NIPAM)$_{45}$ conjugate. B: PAGE analysis of the purified s2-poly(NIPAM)$_{45}$ conjugate. Lane 1 – s2 DNA. Lane 2 – s2-poly(NIPAM)$_{45}$ conjugate.

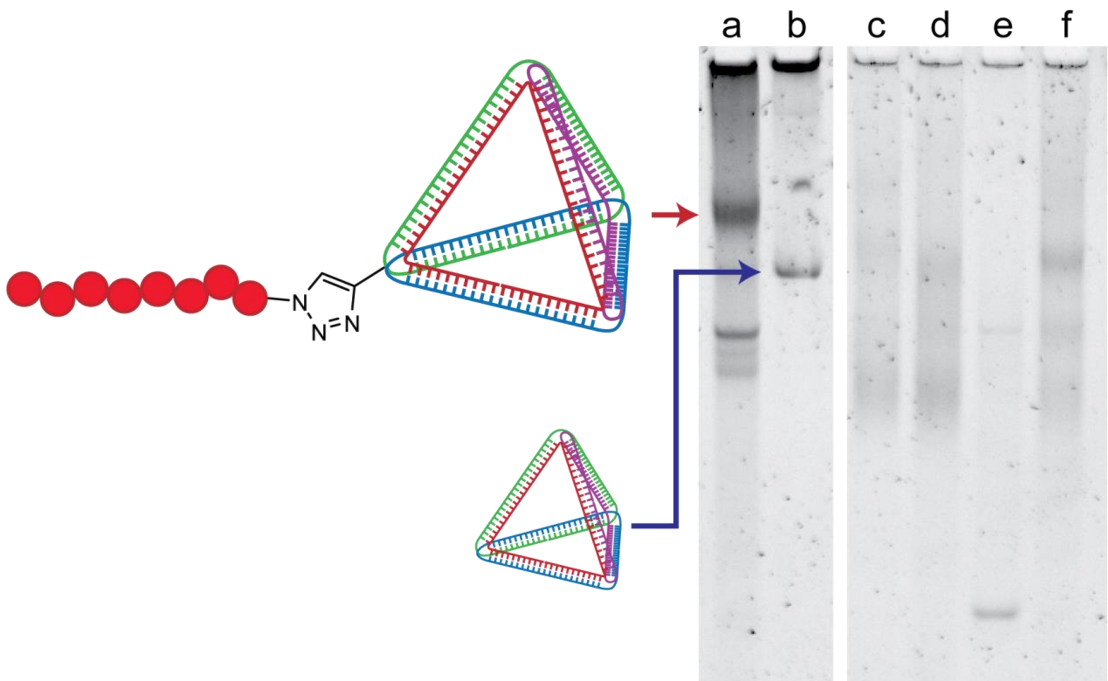

Figure S11. 8 % native PAGE showing that the tetrahedron-polymer conjugate band is only formed when all four constituent DNA strands are present. Lane a: Tetrahedron-poly(NIPAM)$_{45}$ conjugate; lane b: plain tetrahedron; lane c: s1 + s2-poly(NIPAM)$_{45}$ + s3; lane d: s1 + s2-poly(NIPAM)$_{45}$ + s4; lane e: s1 + s3 + s4; lane f: s2-poly(NIPAM)$_{45}$ + s3 + s4.

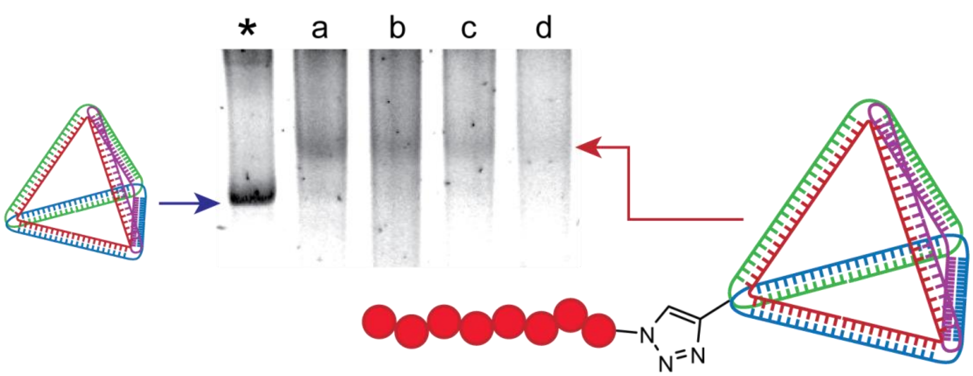

Figure S12. 8 % native PAGE analysis of the tetrahedron-poly(NIPAM)$_{45}$ conjugate incorporating FAM and/or TAMRA. Lane: * – s1-4; a – s1, s2- poly(NIPAM)$_{45}$, s3, s4; b – s1-FAM, s2- poly(NIPAM)$_{45}$, s3, s4; c – s1, s2- poly(NIPAM)$_{45}$, s3-TAMRA, s4; d – s1-FAM, s2-poly(NIPAM)$_{45}$, s3-TAMRA, s4.

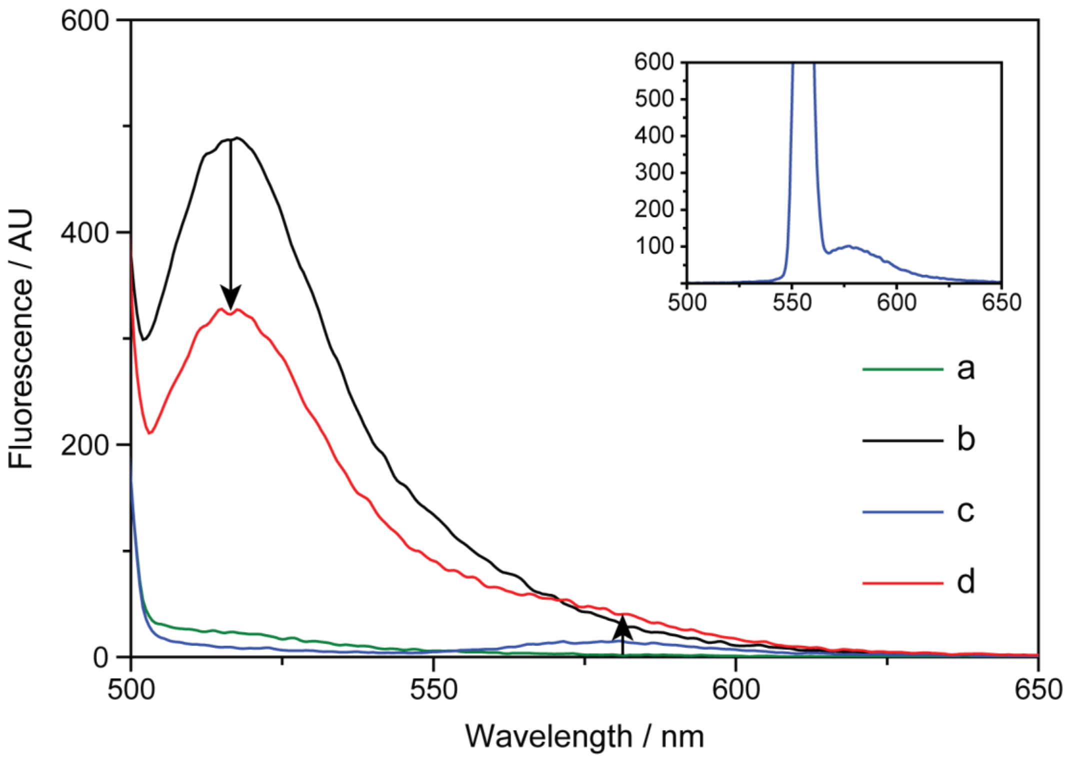

Figure S13. Fluorescence emission spectra of the fluorophore-functionalized tetrahedron-poly(NIPAM)$_{45}$ conjugates, exciting at 495 nm. The experiment labels are the same as those used in Figure S12. Inset: fluorescence emission spectrum of experiment c, exciting at 559 nm to show the presence of the TAMRA group.

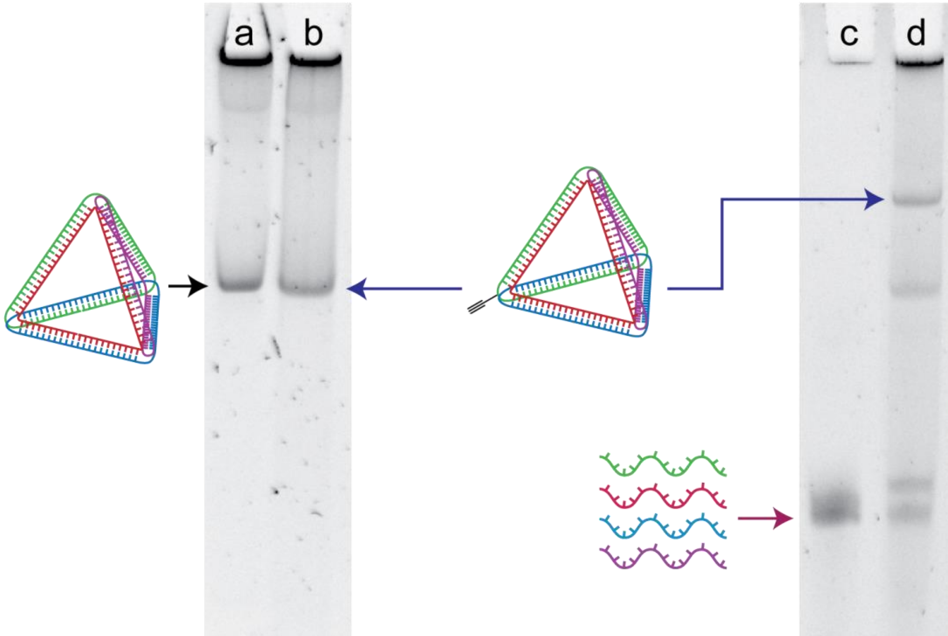

Figure S14. 8 % native (left) and denaturing (right) PAGE analyses of ligated DNA tetrahedra. Lanes a and c contain unligated DNA tetrahedra and lanes b and d ligated tetrahedra. The ligated tetrahedra resisted degradation under denaturing conditions, while the unligated tetrahedra dissociated to the component DNA strands.

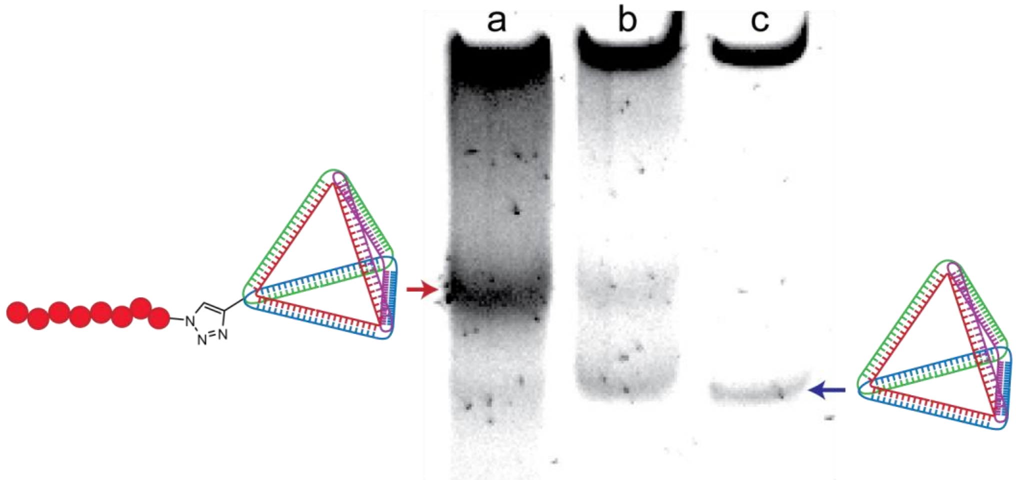

Figure S15. Tetrahedron-PNIPAM$_{45}$ conjugate analyzed by 8 % native PAGE. Lane a: Tetrahedron-PNIPAM$_{45}$ conjugate synthesized by assembly using the s2-poly(NIPAM)$_{45}$ strand; lane b: Tetrahedron-PNIPAM$_{45}$ conjugate synthesized by conjugation of poly(NIPAM)$_{45}$-N$_3$ to an alkyne-functionalized tetrahedron; lane c: plain DNA tetrahedron.

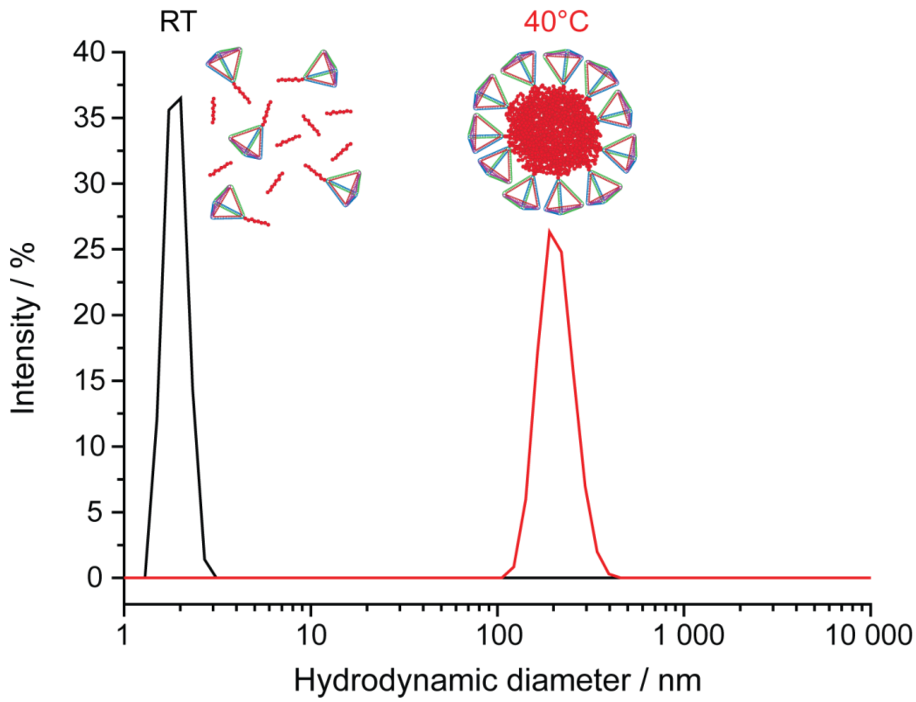

Figure S16. DLS analyses by number of a solution of poly(NIPAM)$_{45}$ and the tetrahedron-poly(NIPAM)$_{45}$ conjugate at room temperature (black) and 40°C (red), showing that the large nanoparticles were only observed at elevated temperatures.

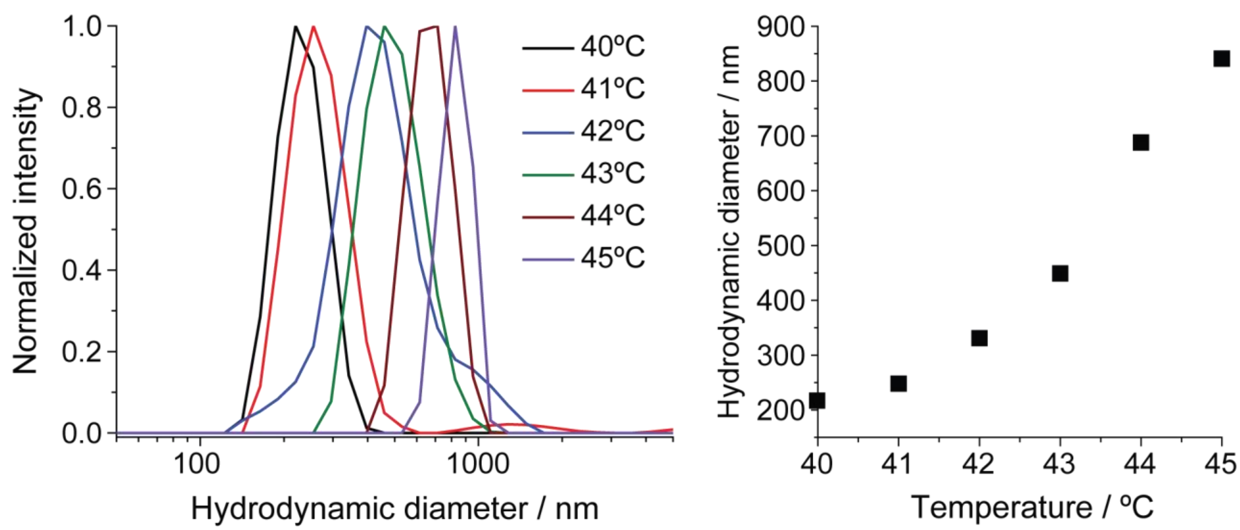

Figure S17. DLS studies of the dependence of the poly(NIPAM)/tetrahedron-poly(NIPAM) nanoparticle size on temperature. Left: DLS intensity traces. Right: plot of the particle size by DLS versus temperature.

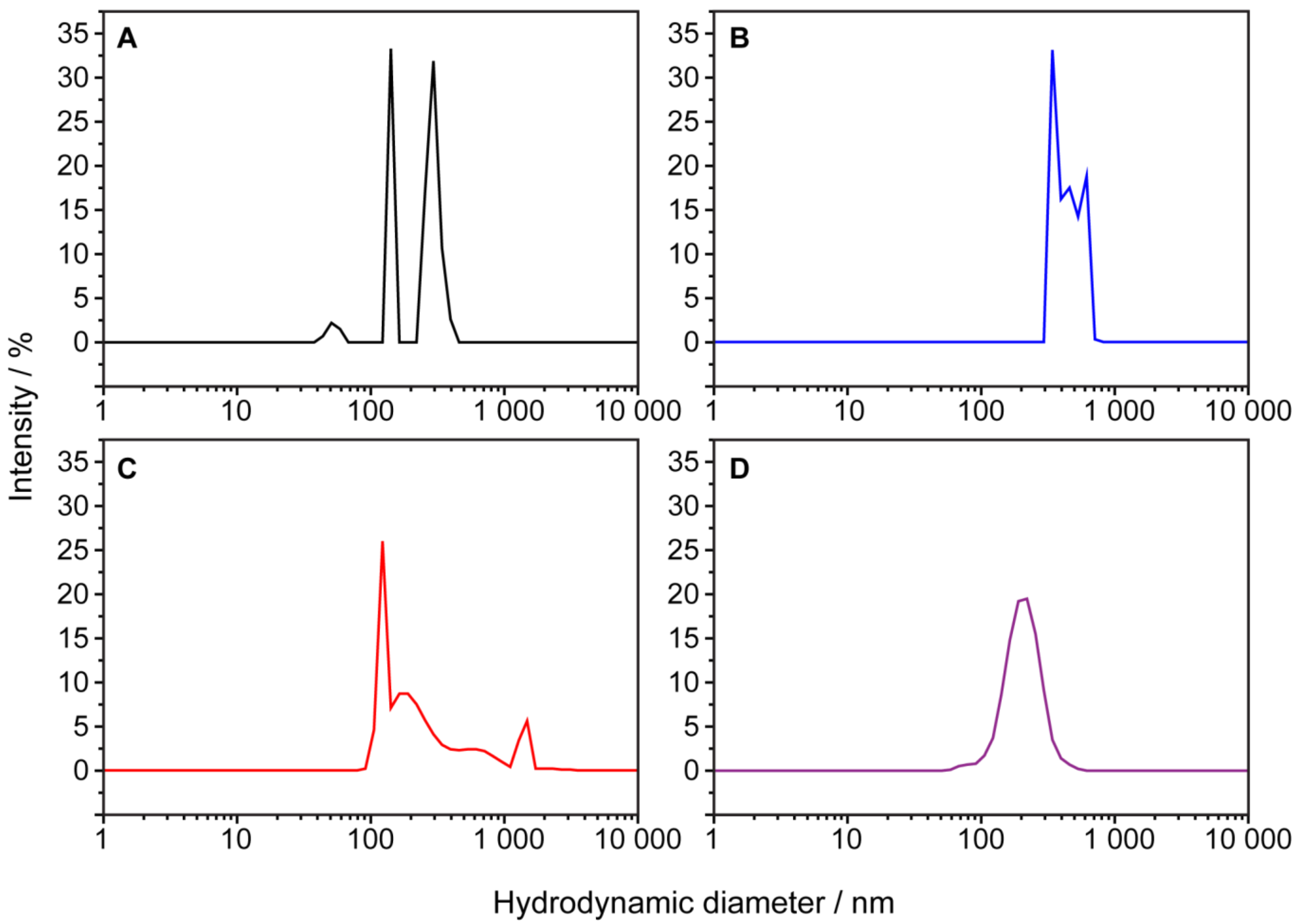

Figure S18. DLS analysis by intensity of solutions of the following in 1 × TEM buffer: **A** – poly(NIPAM)$_{45}$; **B** – poly(NIPAM)$_{45}$ + s2-poly(NIPAM)$_{45}$; **C** - poly(NIPAM)$_{45}$ + plain DNA tetrahedron; **D** - poly(NIPAM)$_{45}$ + DNA tetrahedron-poly(NIPAM)$_{45}$ conjugate. Stable nanoparticles were only observed in the presence of the DNA tetrahedron-polymer conjugate.

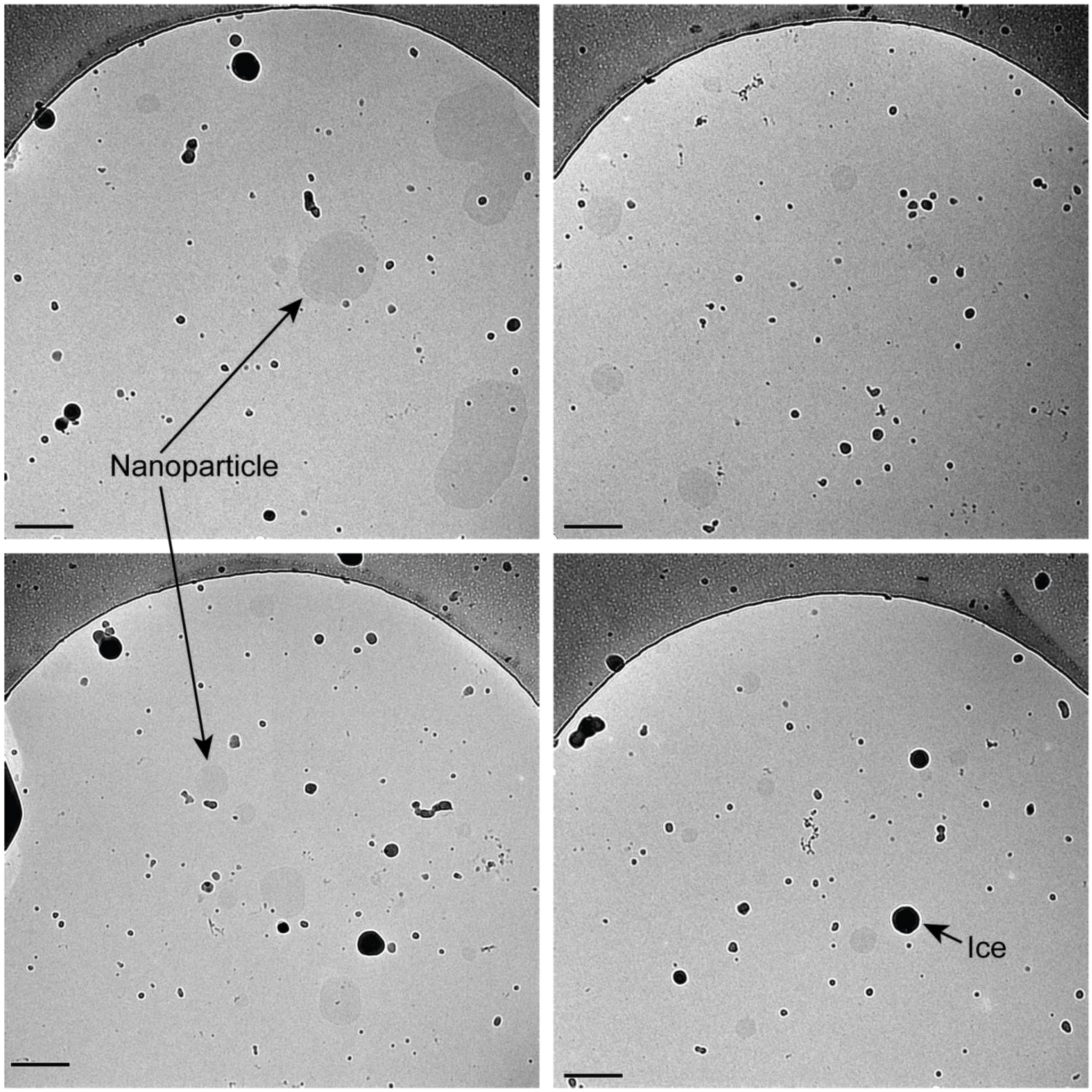

Figure S19. CryoTEM images showing the hybrid DNA tetrahedron-polymer nanoparticles. All scale bars are 200 nm.

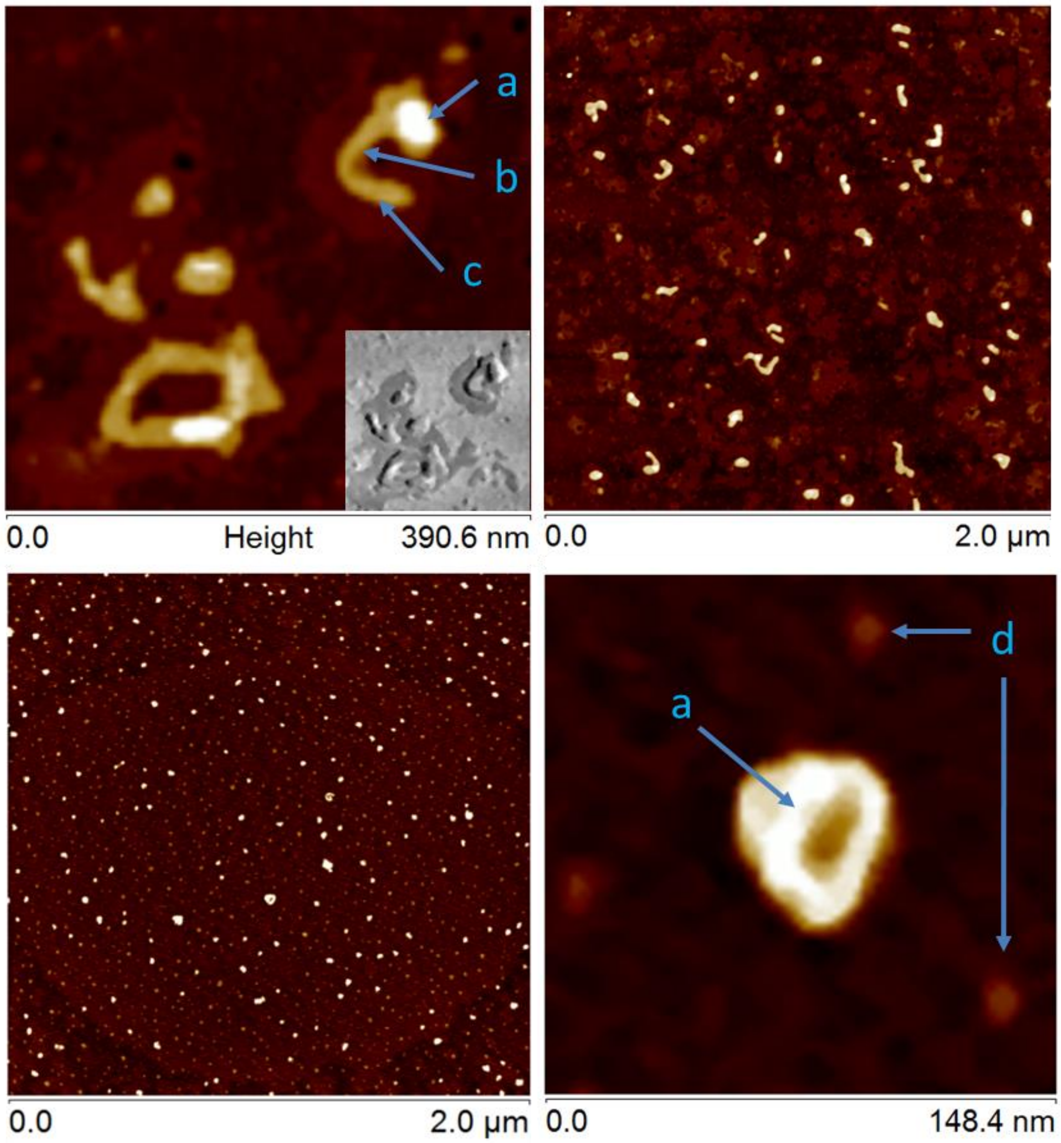

Figure S20. Representative AFM topography micrographs of the hybrid DNA tetrahedron-polymer nanoparticles. Top: spin coated on glass (phase contrast) inset. Bottom: spin coated on mica. Structural assignments: (a) DNA tetrahedron conjugate aggregate - tightly bound, (b) associated poly(NIPAM), (c) associated poly(NIPAM) - collapsed onto surface, and (d) individual DNA tetrahedron-polymer conjugates.

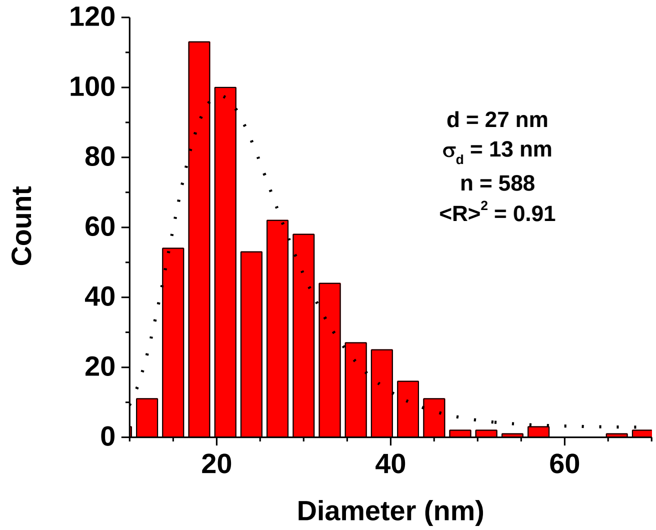

Figure S21. Particle analysis of DNA tetrahedron conjugate aggregates on freshly cleaved mica by AFM. Log-normal fitting of histogram data provided as overlay (---).